Understanding the Low-Frequency Quasilocalized Modes in Disordered Colloidal Systems

Peng Tan,[1] Ning Xu,[2] Andrew B. Schofield,[3] and Lei Xu[1]

[1]*Department of Physics, The Chinese University of Hong Kong, Hong Kong, People's Republic of China*
[2]*Hefei National Laboratory for Physical Sciences at the Miscroscale, CAS Key Laboratory of Soft Matter Chemistry, and Department of Physics, University of Science and Technology of China, Hefei 230026, People's Republic of China*
[3]*The School of Physics, University of Edinburgh, Edinburgh EH9 3 JZ, United Kingdom*

(Received 7 November 2011; revised manuscript received 9 January 2012; published 27 February 2012)

In disordered colloidal systems, we experimentally measure the normal modes with the covariance matrix method and clarify the origin of low-frequency quasilocalization at the single-particle level. We observe important features from both jamming and glass simulations: There is a plateau in the density of states [$D(\omega)$] which is suppressed upon compression, as predicted by jamming; within the same systems, we also find that the low-frequency quasilocalization originates from the large vibrations of defective structures coupled with transverse excitations, consistent with a recent glass simulation. The coexistence of these features demonstrates an experimental link between jamming and glass. Extensive simulations further show that such a structural origin of quasilocalization is universally valid for various temperatures and volume fractions.

DOI: 10.1103/PhysRevLett.108.095501 PACS numbers: 63.50.−x, 63.20.kp, 71.55.Jv

One important unsolved problem in condensed matter physics is the existence and properties of anomalous low-frequency modes in disordered systems, which often form the broad boson peak in the $D(\omega)/\omega^{d-1}$ spectrum (d is the dimension of space). A number of models have attributed the anomalies to a soft potential [1], evolution from a van Hove singularity [2], transition from a minima-dominated phase to a saddle-point-dominated phase [3], and the Ioffe-Regel limit [4]. Although these modes are generally accepted to be quasilocalized [5–8], their origin remains open to debate. In simulations of jammed packings of frictionless spheres, the jamming transition produces a plateau in $D(\omega)$, which is suppressed by compression and leads to quasilocalized modes [9–15]. A recent simulation in model glasses demonstrates that the low-frequency quasilocalized modes come from the coupling between large vibrations of defective soft regions and transverse excitations [16]. Despite these important results, however, experimental test is lacking, and a possible connection between different models is also missing. Using colloidal systems, we directly probe the low-frequency quasilocalized modes at the single-particle level. The origin observed in our experiment is consistent with both jamming and glass simulations, demonstrating a direct link between the two important models. Extensive simulations further show that our result is universally valid for various temperatures and volume fractions.

We prepare 2D samples by suspending a single layer of poly(methyl methacrylate) particles with diameter $a = 2.0\ \mu$m (polydispersity $<3\%$) between two glass substrates. The particles are suspended in the mixture of iododecane and iodododecane (volume ratio 1:4), forming density and refractive-index matched systems. The particles and glass substrates are both coated with polyhydroxystearic acid polymers and carry the same type of charges in the weakly polar solvent. They interact with the long-range repulsive Yukawa potential (the screening length is 0.975 μm in the low-concentration limit). Since there is no particle-particle and particle-wall contact, we completely eliminate the effect from contact frictions [17]. Using confocal microscopy, we track every particle's motion with a spatial resolution of 15 nm, at the frame rate of 30 s^{-1}. In each sample, we track all particles within the field of view for 2000 frames and calculate the normal modes by diagonalizing the covariance matrix: $C_{i,j} = \langle[\mathbf{r}_i(t) - \langle\mathbf{r}_i(t)\rangle][\mathbf{r}_j(t) - \langle\mathbf{r}_j(t)\rangle]\rangle$ $(i, j = 1, \ldots, 2N$ run over the x and y coordinates of N particles, and $\langle\,\rangle$ means time average over all frames). The eigenvectors give the polarization vectors of the normal modes; and the eigenvalues $\lambda = k_BT/m\omega^2$ yield the angular frequencies ω [6–8]. This method is valid for stable and metastable systems, in which no particle should rearrange; we therefore check every frame to make sure no rearrangement occurs during the entire process. Within the measurement time, every particle moves around its equilibrium position and the system is metastable, while for longer times, thermal motions cause rearrangements and the system relaxes, which may introduce anomalies for low-frequency mode calculation. Thus, the relaxation limits our measurement time to 2000 frames.

To quantitatively describe the individual particle's local environment, we directly measure each particle's local bond orientational order parameter $\Psi_{6i} = \frac{1}{n_i}|\sum_{m=1}^{n_i} e^{j6\theta_{mi}}|$, determined by the particle's nearest-neighbor arrangement. Here n_i is the number of nearest neighbors around particle i, and θ_{mi} is the angle between $\mathbf{r}_m - \mathbf{r}_i$ and the x axis. $\Psi_{6i} = 1$ means perfect hexagonal arrangement of six

nearest neighbors, and $\Psi_{6i} = 0$ means totally random arrangement. We use different colors to represent different Ψ_{6i} values in Fig. 1(a). Possibly due to nonuniform charges, all samples are heterogeneous, with Ψ_{6i} ranging from 0 to 1. We can also systematically decrease the overall amount of disorder by increasing the number density, as shown by the evolution from amorphous to polycrystalline samples in Fig. 1(a).

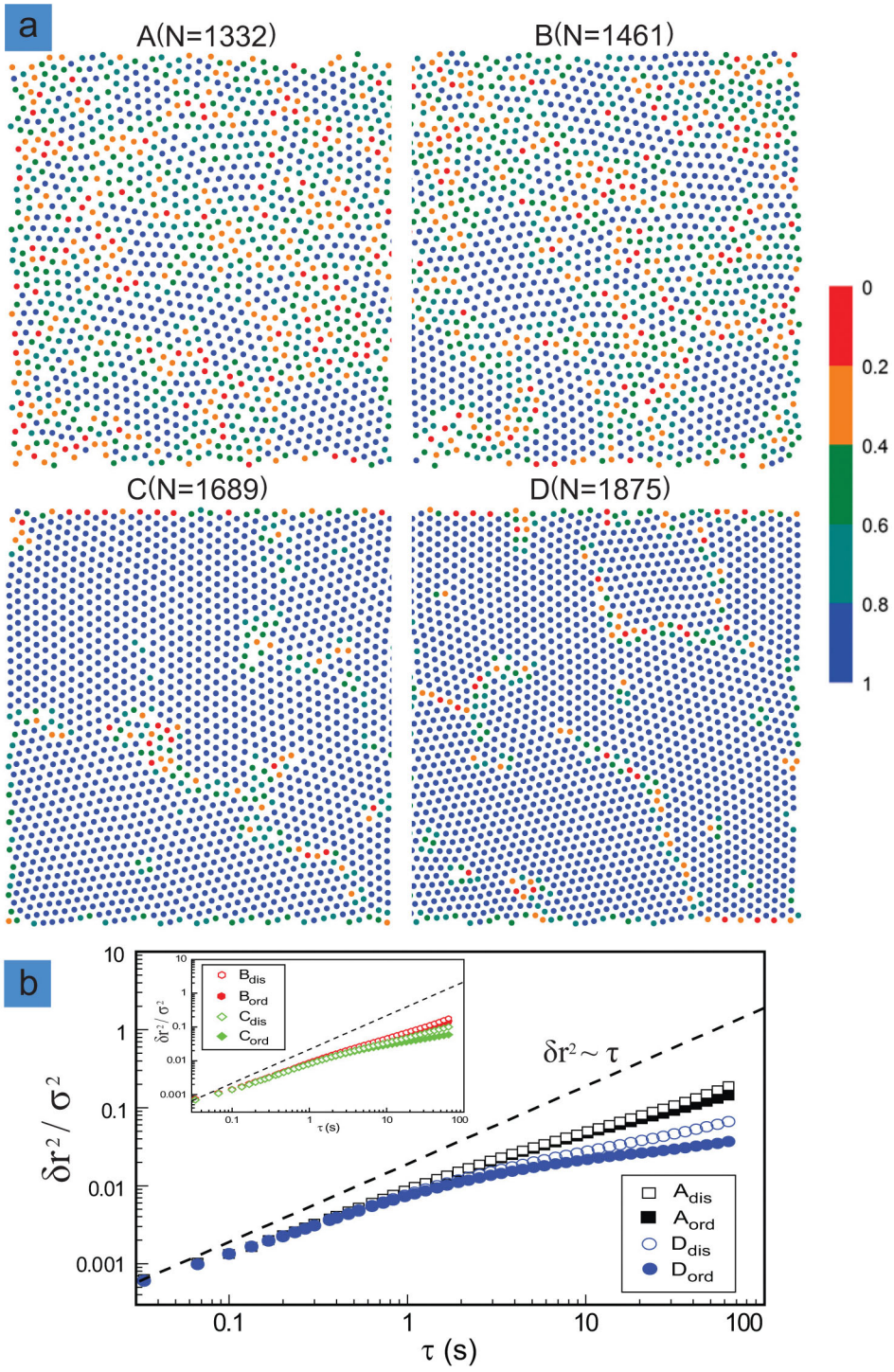

FIG. 1 (color online). The structures and MSD of four typical samples. (a) From *A* to *D*, the samples vary from amorphous to polycrystalline with compression. The total dimensions are 146×146 μm^2. Different colors correspond to different Ψ_{6i} values. (b) MSD curves for the disordered particles (open symbols) and ordered particles (solid symbols) in *A* and *D*. Higher MSD of disordered particles demonstrates their larger motions. All curves are below the dashed line of free diffusion, as the result of caging. *B* and *C* are shown in the inset.

Within each system, we divide particles into two groups: the disordered particles with Ψ_{6i} less than the system average ($\Psi_{6i} < \bar{\Psi}_{6i}$) and the ordered particles with Ψ_{6i} larger than the system average ($\Psi_{6i} > \bar{\Psi}_{6i}$). This helps to identify the roles of each group, especially the disordered group, in the formation of low-frequency quasilocalized modes. Figure 1(b) (main panel) shows the mean square displacement (MSD) for disordered particles (labeled as "dis") and ordered particles (labeled as "ord") in samples A and D (B and C are shown in the inset). The MSD for disordered particles is higher than that for ordered ones, indicating qualitatively larger movements of disordered particles. In addition, all MSD curves increase slower than the dashed line of free diffusion, as the result of caging. To make sure that the slowly rising MSD does not affect the calculation of low-frequency normal modes, we compare the experimental results with flat-MSD simulations in Fig. 4. Their agreement confirms the reliability of our results.

The density of states $D(\omega)$ is plotted in Fig. 2(a). For each curve, we can clearly identify a plateau, which shrinks upon the compression from A to D. This observation agrees well with the special feature of jammed packings of frictionless spheres: A plateau develops in $D(\omega)$, which extends to $\omega = 0$ at the unjamming transition [10]. To the best of our knowledge, no plateau in $D(\omega)$ has ever been observed in other colloidal experiments. We suspect that it is due to the absence of contact friction in our system [17]. Other factors, such as temperature, number density, and interaction potential, could also be relevant. In the inset, a peak shows up in the $D(\omega)/\omega$ spectrum for samples C and D and probably shifts to lower frequencies for A and B (not resolved in our experiment). This is again consistent with the jamming result: The boson peak shifts to lower frequencies for less compressed systems [10]. A similar result was also observed experimentally [7].

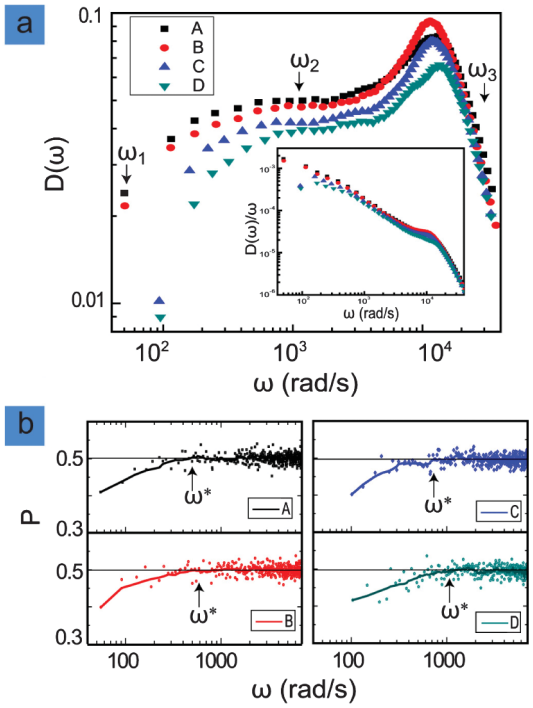

FIG. 2 (color). The density of states and participation ratio of the normal modes. (a) The density of states $D(\omega)$ of the four samples. In each curve, we can identify a plateau, which shrinks with compression from A to D, consistent with the jamming prediction. The inset shows the $D(\omega)/\omega$ spectrum. (b) The participation ratio P at different frequencies. The solid curves are the smoothed results of data. At small ω, the modes are quasilocalized with small P values, while after the characteristic frequency ω^*, P reaches a stable value. ω^* increases with compression.

To verify the quasilocalization of the low-frequency modes, we plot the participation ratio P in Fig. 2(b) and observe the following behaviors: (i) At low frequencies, the modes are quasilocalized with small P values increasing progressively; (ii) after this low-frequency regime, the modes become extended with large and stable P; (iii) the transition frequency where P first becomes stable, ω^*, increases with the compression. All these behaviors agree with jammed solids at $T = 0$ [10–12,15], demonstrating the connection between our experiment and jamming.

For a detailed understanding of normal mode structures, we analyze the polarization vectors at the single-particle level. Figure 3(a) shows three typical modes, $\omega_1 < \omega_2 < \omega_3$, in sample A [exact location shown in Fig. 2(a)]. The low-frequency mode ω_1 vibrates collectively with large-scale correlations, while ω_2 and ω_3 look rather random. Further inspection on ω_1 reveals that large-amplitude vibrations mostly occur at disordered sites. To quantitatively verify this, we compute the mean square vibration amplitude of disordered particles, $\overline{A^2_{\rm dis}}$, and ordered particles, $\overline{A^2_{\rm ord}}$. Their ratio $\overline{A^2_{\rm dis}}/\overline{A^2_{\rm ord}}$ reflects the relative vibrational strength between the two groups of particles, as plotted in Fig. 3(c). In all samples, $\overline{A^2_{\rm dis}}/\overline{A^2_{\rm ord}}$ is larger than 1 at small ω but drops to unity as ω increases. This quantitatively proves that disordered particles vibrate stronger than ordered ones at low frequencies, as suggested in the recent simulation of glasses [16]. Moreover, the transition frequency $\omega^\dagger$, where $\overline{A^2_{\rm dis}}/\overline{A^2_{\rm ord}}$ first systematically reaches unity, agrees with ω^* in Fig. 2(b). This indicates that the quasilocalized modes below ω^* come from large-amplitude vibrations at *disordered or soft* sites under $\omega^\dagger$. These large vibrations at soft sites may also explain the recent discovery of correlations between low-frequency modes and particle rearrangements [18,19].

While the polarization vectors in real space reveal the locations of large vibrations, their Fourier transform in q space brings further insights. In Fig. 3(b), we decompose ω_1, ω_2, and ω_3 into transverse and longitudinal Fourier components and illustrate them within the first Brillouin zone. The two components are defined as

$$f_{\omega,tr}(\mathbf{q}) = |\Sigma_i(\hat{\mathbf{q}} \times \mathbf{e}_{i,\omega}) \exp(i\mathbf{q} \cdot \mathbf{r}_i)|^2, \qquad (1)$$

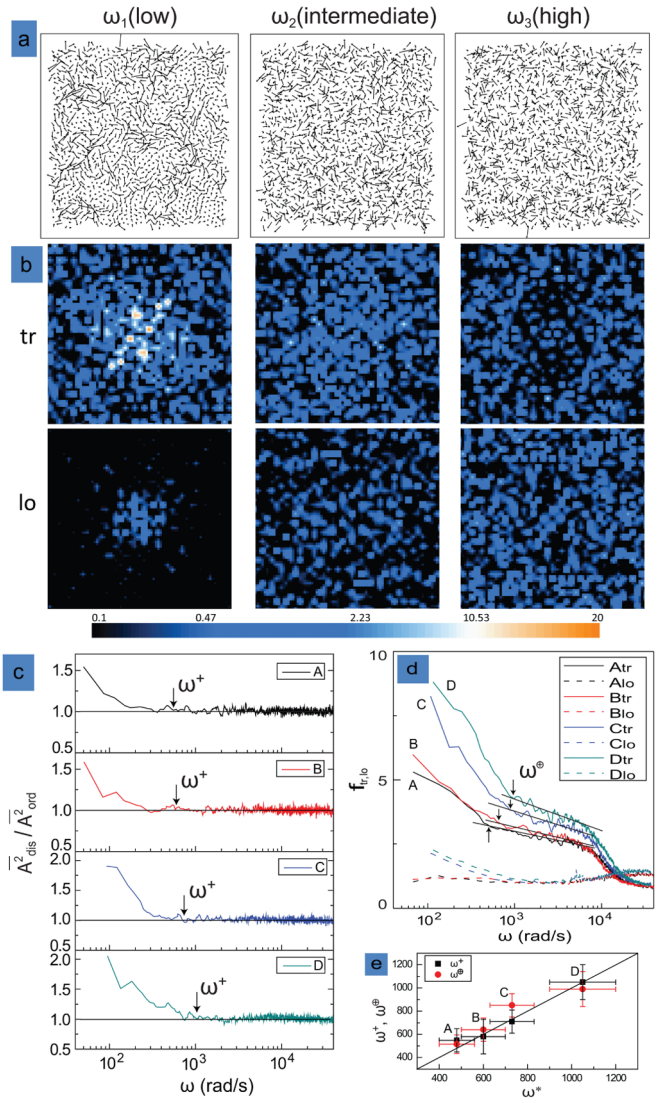

FIG. 3 (color online). Vibration distribution in real and Fourier spaces. (a) The polarization vectors of three typical modes, $\omega_1 < \omega_2 < \omega_3$, in sample A. The low-frequency mode (ω_1) has large-scale collective correlations, while the other two (ω_2 and ω_3) look random. (b) The transverse and longitudinal Fourier components of the three modes within the first Brillouin zone. At ω_1, the long-wavelength transverse component dominates. (c) The ratio of the mean squared vibration amplitude between disordered particles and ordered particles, $\overline{A^2_{\rm dis}}/\overline{A^2_{\rm ord}}$. It is initially larger than 1 but drops to unity after the transition frequency $\omega^\dagger$. (d) The average magnitude of transverse and longitudinal components of all samples. The average is taken over the small q area $[-\frac{\pi}{2\sigma} < q_x, q_y < \frac{\pi}{2\sigma}]$. The transverse curves (solid) dominate the longitudinal ones (dashed) at low frequencies. Each transverse curve contains a plateau with the onset frequency $\omega^\oplus$, as illustrated by the arrows. (e) The agreement of ω^*, $\omega^\dagger$, and $\omega^\oplus$.

$$f_{\omega,lo}(\mathbf{q}) = |\Sigma_i(\hat{\mathbf{q}} \cdot \mathbf{e}_{i,\omega}) \exp(i\mathbf{q} \cdot \mathbf{r}_i)|^2. \quad (2)$$

Here $\mathbf{e}_i$ and $\mathbf{r}_i$ are the polarization vector and position vector, respectively, of particle i. The summation is over all particles.

We first focus on the low-frequency mode at ω_1: The transverse component has much larger overall magnitude and dominates the longitudinal one, verifying the transverse nature of the low-frequency modes [16]. Moreover, the large magnitude concentrates on small q values, indicating long-wavelength transverse excitations. At the intermediate frequency ω_2, the transverse component distributes more uniformly. At even higher frequency ω_3, the transverse component decreases dramatically at small q, making its small-q magnitude less than the high-q magnitude. By contrast, the longitudinal component keeps spreading in q space as ω increases.

To illustrate the overall evolution of the transverse and longitudinal components, we plot their average magnitude at different frequencies in Fig. 3(d). At low frequencies, the transverse curves dominate the longitudinal ones, consistent with Fig. 3(b). More interestingly, each transverse curve also contains a plateau with an onset frequency $\omega^\oplus$, which matches ω^* and $\omega^\dagger$. Their agreement in Fig. 3(e) indicates that multiple distinctive changes occur around the same frequency.

Combining the measurements of local environment and vibrational properties at the single-particle level, we find that low-frequency quasilocalized modes are caused by collective large vibrations at disordered sites, coupled with long-wavelength transverse excitations. This is consistent with a recent simulation of model glasses [16]. Moreover, the characteristic frequencies present in model glasses ($\omega^\dagger$) and jammed packings of frictionless spheres (ω^*) agree well with each other, providing an experimental link between the two important models.

Some special features of jammed solids near the jamming transition emerge in our colloidal experiment. How can the jamming transition, defined at $T = 0$, influence our finite temperature experiment? To understand it, we perform numerical simulations for both thermal ($T > 0$) and athermal ($T = 0$) systems, at different volume fractions ϕ. We use the Yukawa potential which is consistent with experiments. At $T = 0$, we use low-memory Broyden-Fletcher-Goldfarb-Shanno quasi-Newtonian minimizer energy minimization to generate packings and obtain normal modes from the Hessian matrix. At $T > 0$, we perform molecular dynamics simulations and diagonalize the covariance matrix to get normal modes. The different conditions are represented by different shapes (for T) and colors (for ϕ) in Fig. 4(a). The solid and open symbols represent systems with and without, respectively, the typical jamming feature—a plateau in $D(\omega)$. At $T = 0$, the plateau shrinks with increasing volume fraction and eventually disappears, consistent with previous simulations [10]. Interestingly, such a feature persists at $T > 0$ but moves to higher ϕ for higher T. We suspect that the existence of the plateau at $T > 0$ is the *vibrational* thermal vestige of the zero temperature jamming transition [5], which is responsible for the experimentally observed plateau.

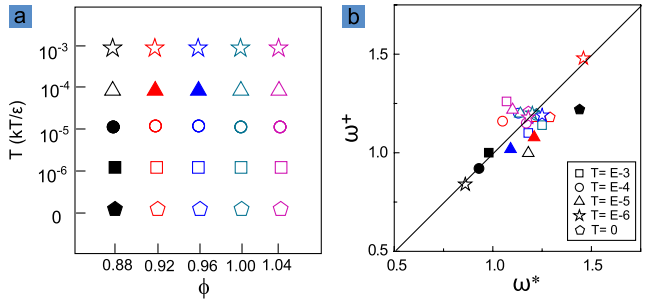

FIG. 4 (color online). Simulations at various temperatures and volume fractions. (a) Different conditions represented by different shapes (for T) and colors (for ϕ). The solid and open symbols represent systems with and without a plateau in $D(\omega)$, respectively. (b) The comparison of $\omega^{\dagger}$ and ω^{*} determined by $\overline{A^2_{\mathrm{dis}}}/\overline{A^2_{\mathrm{ord}}}$ and P, respectively. Reasonable agreement appears in all samples, suggesting that the correspondence between the low-frequency quasilocalization and large vibrations at disordered sites is universal.

Regardless of the shape of $D(\omega)$, the correspondence between the low-frequency quasilocalization and the large vibrations at disordered sites appears in all simulations. The agreement of ω^{*} and $\omega^{\dagger}$ for all conditions is illustrated in Fig. 4(b). Therefore, the structural origin of the quasilocalization observed experimentally may be universal for amorphous systems at different T and ϕ.

Using colloidal systems, we experimentally demonstrate that the low-frequency quasilocalization originates from large vibrations of disordered structures, coupled with long-wavelength transverse excitations. The general features of both jamming and glass models coexist in our experiment, suggesting possible links between the two. Our simulation further suggests the possible existence of a vibrational thermal vestige for the jamming transition.

We thank Sidney Nagel, Andrea Liu, Carolina Brito, and Jiping Huang for helpful discussions. P. T. and L. X. are supported by Hong Kong RGC (GRF CUHK404211 and direct Grant No. 2060395) and UGC (SEG—CUHK07). N. X. is supported by National Basic Research Program of China (973 Program) No. 2012CB821500 and National Natural Science Foundation of China (No. 91027001).

[1] M. I. Klinger, Phys. Rep. **94**, 183 (1983).
[2] W. Schirmacher, G. Diezemann, and C. Ganter, Phys. Rev. Lett. **81**, 136 (1998).
[3] T. Grigera, V. Martn-Mayor, G. Parisi, and P. Verrocchio, Nature (London) **422**, 289 (2003).
[4] H. R. Schober, J. Phys. Condens. Matter **16**, S2659 (2004).
[5] Z. Zhang *et al.*, Nature (London) **459**, 230 (2009).
[6] A. Ghosh *et al.*, Phys. Rev. Lett. **104**, 248305 (2010).
[7] K. Chen *et al.*, Phys. Rev. Lett. **105**, 025501 (2010).
[8] D. Kaya, N. L. Green, C. E. Maloney, and M. F. Islam, Science **329**, 656 (2010).
[9] A. J. Liu and S. R. Nagel, Nature (London) **396**, 21 (1998).
[10] L. E. Silbert, A. J. Liu, and S. R. Nagel, Phys. Rev. Lett. **95**, 098301 (2005).
[11] M. Wyart, S. R. Nagel, and T. A. Witten, Europhys. Lett. **72**, 486 (2005).
[12] M. Wyart *et al.*, Phys. Rev. E **72**, 051306 (2005).
[13] N. Xu, V. Vitelli, M. Wyart, A. J. Liu, and S. R. Nagel, Phys. Rev. Lett. **102**, 038001 (2009).
[14] V. Vitelli *et al.*, Phys. Rev. E **81**, 021301 (2010).
[15] N. Xu, V. Vitelli, A. J. Liu, and S. R. Nagel, Europhys. Lett. **90**, 56 001 (2010).
[16] H. Shintani and H. Tanaka, Nature Mater. **7**, 870 (2008).
[17] E. Somfai *et al.*, Phys. Rev. E **75**, 020301(R) (2007).
[18] K. Chen *et al.*, Phys. Rev. Lett. **107**, 108301 (2011).
[19] M. L. Manning and A. J. Liu, Phys. Rev. Lett. **107**, 108302 (2011).